The 2020 World Congress on
Advances in Civil, Environmental, & Materials Research (ACEM20)
25-28, August, 2020, GECE, Seoul, Korea

Dynamic calibration of drag balance using finite element analysis

*Keunyeong Kim[1)], Byungkook Jang[2)] and Gisu Park[3)]

[1), 2), 3)] Department of Aerospace Engineering, KAIST, Daejeon 34141, Republic of Korea
[1)] scorpius_a@kaist.ac.kr
[2)] bk_jang@kaist.ac.kr
[3)] gisu82@kaist.ac.kr

ABSTRACT

In this study, a drag balance was studied using the stress wave force balance technique to measure the drag in a shock tunnel, which had a test time in the order of milliseconds. The dynamic calibration of the balance was performed through finite element analysis. The system responses induced by the applied loads of various shapes and amplitudes were simulated, and the impulse response function was determined through deconvolution processes. The drag recoveries were performed using the impulse response function of the system. The factors that should be considered in the recovery process are summarized.

1. INTRODUCTION

The stress wave force balance is one of the techniques used for measuring aerodynamic forces, in which the test time is in the order of milliseconds (Sanderson and Simmons 1991). When an aerodynamic load is suddenly applied to the system, stress waves are generated, propagated, and reflected, which induces local deformation and vibration in the system. The stress wave force balance is used to analyze this stress wave behavior and recover the applied load from the vibrating strain signals using inverse techniques. Therefore, it is necessary to determine the dynamic response characteristics of the system accurately through dynamic calibration.

In this study, finite element analysis was applied to simulate the behavior of the stress wave force balance for drag measurements, and the dynamic response characteristics of the system corresponding to forces of various shapes and amplitudes were obtained. The simulated aerodynamic load in the test facility was recovered using the obtained dynamic response characteristics. Furthermore, a summary of the findings obtained for the dynamic calibration process is presented in this paper.

For a linear time invariable system, the dynamic behavior of the system can be modeled using a convolution integral (Sanderson and Simmons 1991~Vadassery et al.

[1,2)] Graduate Student
[3)] Associate Professor, Corresponding author

2013). For the stress wave force balance, y, u, and g denote the measured strain signal, applied external force and impulse response function of the system, respectively.

$$y(t) = \int_0^t g(t-\tau)u(\tau)d\tau \quad (1)$$

If the impulse response function of a system is known, the applied external forces can be recovered through deconvolution between the measured strain signal and impulse response function. The impulse response function of the system is determined through dynamic calibration. External forces having known shapes and amplitudes, such as a pulse load applied using an impact hammer, are applied to the system to determine the impulse response function of the system. The impulse response function can be obtained through deconvolution between the force input history and the resulting strain signal. As the impulse response function is determined using the deconvolution technique, slight errors can accumulate over time resulting in a significant error in the force recovery process. Therefore, in this study, the least square deconvolution method was utilized instead of the simple deconvolution based on Laplace transformation (Mee 2003a, Mee 2003b).

2. DRAG BALANCE

Fig. 1 shows the schematic of the stress wave force balance used in this study for measuring the drag. The balance was designed for performing drag measurement in a K1 shock tunnel, consisted of a test model, stress bar, fixed-end support, and aerodynamic shield. The shock tunnel consisted of a shock tube, Mach 6 contoured nozzle, test section, and dump tank. Detailed information regarding the shock tube and the shock tunnel can be found in literatures (Park 2013~Kim and Park 2020)

The test model was a simple sharp-pointed circular cone with an 18º semi-nose angle. The entire system was manufactured using a single material, Al-6061. The test model and stress bar were manufactured as a single integrated unit. The aerodynamic shield was applied by wrapping the stress bar to prevent unexpected flow-structure interactions. The entire system was fixed to the test section using the fixed-end support for convenience in the system setup. A semiconductor strain gauge (Model S/UCP-120-090, Kulite) was used to detect micro-level strain with good accuracy and was mounted parallel to the stress bar.

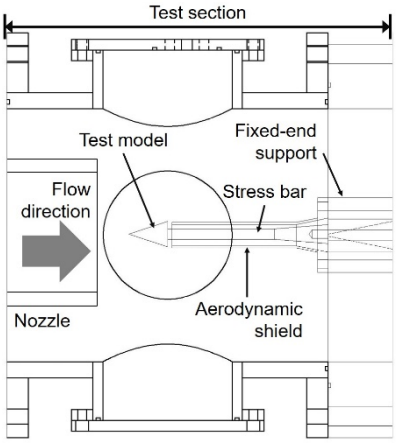

Fig. 1 Schematic of drag balance

3. FINITE ELEMENT ANALYSIS

Finite element analysis was conducted using a commercial transient structural package in ANSYS R16.1. A program-controlled solver was used to perform the linear solution. Tetrahedral and hexahedral elements were utilized to simulate the dynamic behavior of the axis-symmetric parts of the drag balance and fixed support, respectively. A strain gauge was simulated using solid elements created on the surface of the stress bar, and the obtained strain signals from the simulated strain gauge were used for processing. The elemental size at the strain gauge was the smallest to achieve higher accuracy of the strain signal elements. The resulting mesh was generated and contained 208,101 elements. Fig. 2 shows the generated mesh of the drag balance. A fixed support condition was applied to the front and the rear surface of the fixed-ended support to restrict the movement, similar to actual experimental conditions. The external force was applied to the point or surface of the test model.

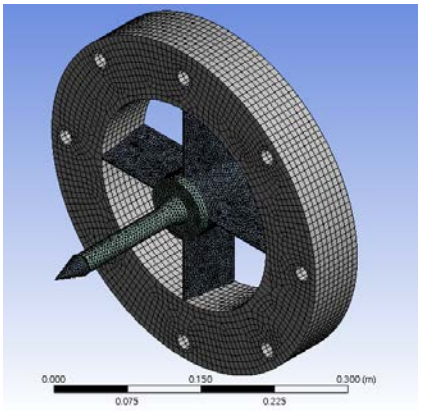

Fig. 2 Computational mesh

3.1 Simulated shock tunnel data

In this study, shock tunnel data was simulated through finite element analysis. Fig. 3 shows the simulated shock tunnel data. Fig. 3a depicts the assumed drag history (hypothetical history) applied to the test model, which was used as input to the finite element analysis. The amplitude and the shape of the drag were assumed arbitrary. Fig. 3b shows the simulated strain at the strain gauge elements corresponding to the drag input depicted in Fig. 3a. The input load was applied to the test model vertex. The simulated strain was assumed to be the strain signal obtained experimentally, and the drag was recovered from the strain.

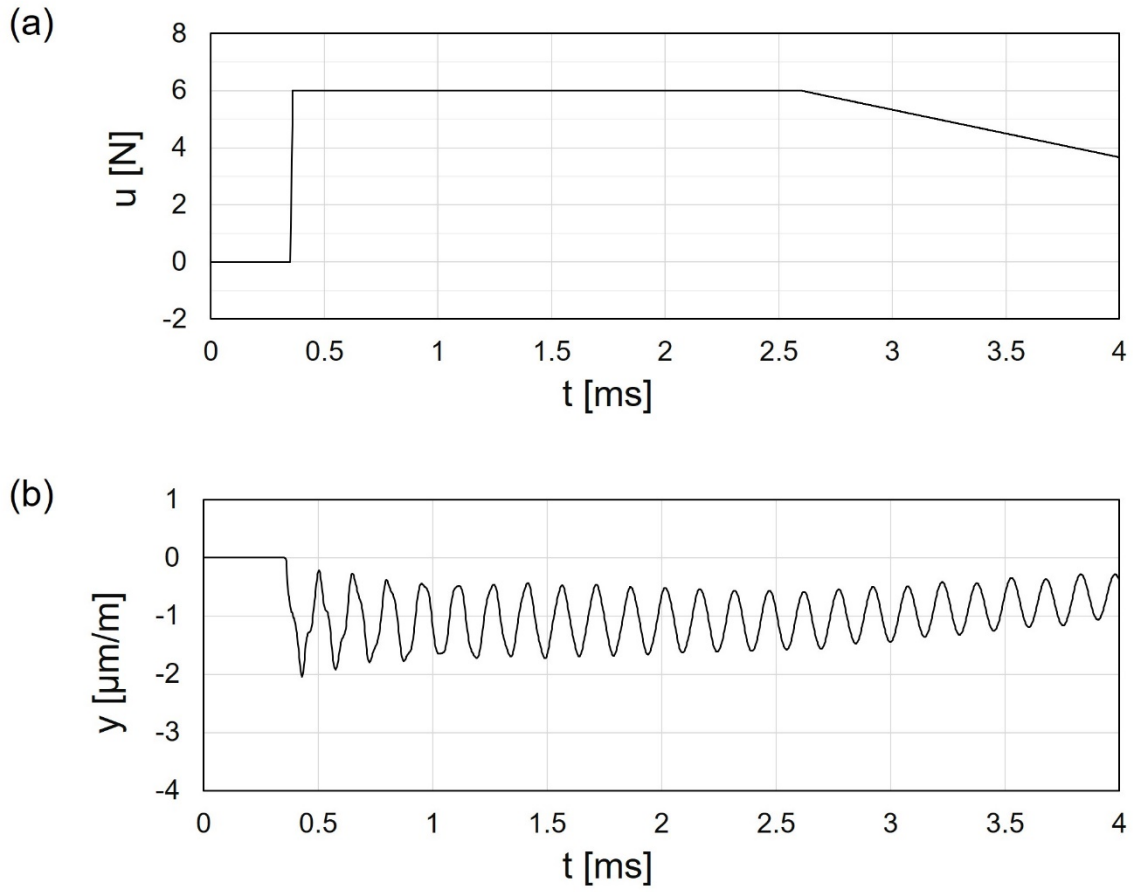

Fig. 3 Simulated shock tunnel data; (a) drag history; (b) strain signal output.

3.2 Recovery using step load

The step load represents the load with a constant level offset after a sudden increase, and the critical parameters of the step load were the load amplitude and rise time. Fig. 4a depicts the step load input for a rising time of 10 μs and the resulting strain signal output. A simple step load with a maximum amplitude of 6 N was applied to the test model vertex.

It was confirmed that the strain signals had an offset of approximately -1 μm/m with high-frequency vibrations. The impulse response functions were determined through the deconvolution process using the results depicted in Fig. 4a, and the obtained functions were used to recover the strain signal in Fig. 3b. In this study, the least square deconvolution algorithm was used to deconvolve the signals (Hu and Milenkovic 1990). Fig. 4b shows the comparison between the original drag and recovered drag, and the differences are insignificant. Significantly extended rise time was observed for the recovered drag compared to the original drag. This trend occurred because of the signal smothering caused by the least square deconvolution process.

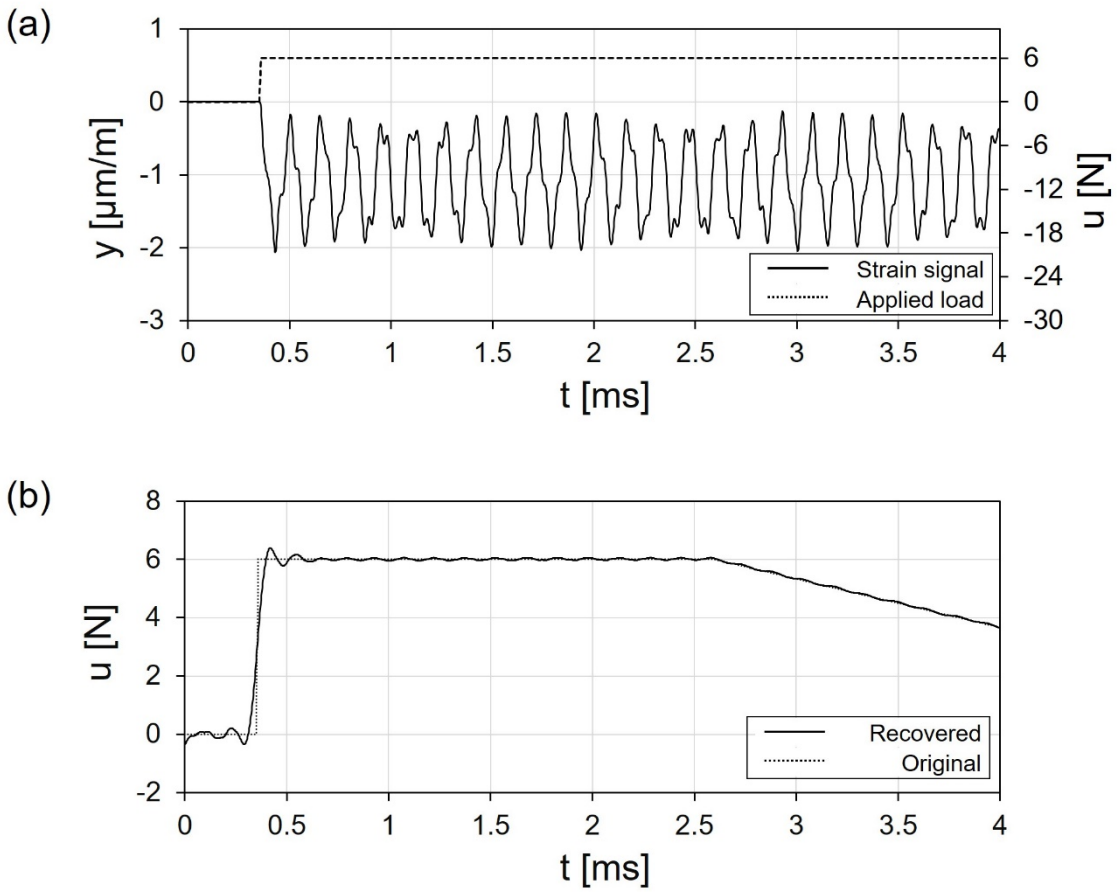

Fig. 4 Drag recovery using step load; (a) step load response; (b) drag comparison.

3.3 Recovery using pulse load

The pulse load represents the load that was applied for only a short duration. The parameters used to describe the pulse load were more than those of the step load, such as the pulse shape, load amplitude, and pulse duration. Fig. 5 shows the simulated results of the pulse input and the drag recovery results. The pulse load shown in Fig. 5a is a sine-shaped load for a pulse duration of 360 μs. The pulse shape obtained from the applied hammer was similar to the sine shape. Therefore, the pulse inputs were modelled as a sine shape. A sine pulse with a maximum amplitude of 0.56 N was applied to the

test model vertex. The impulse response functions were obtained according to the pulse results through the same process as the step loads and recovered drags.

The difference between original and the recovered drags increased with time for the pulse load case. In this case, the load data was concentrated for a significantly shorter period than for step loads. Therefore, the impulse response function for the pulse loads was much sensitive to the deconvolution error (Mee 2003b). The accumulated error (Fig. 5b) possibly originated from the deconvolution errors during the process of determining the impulse response function.

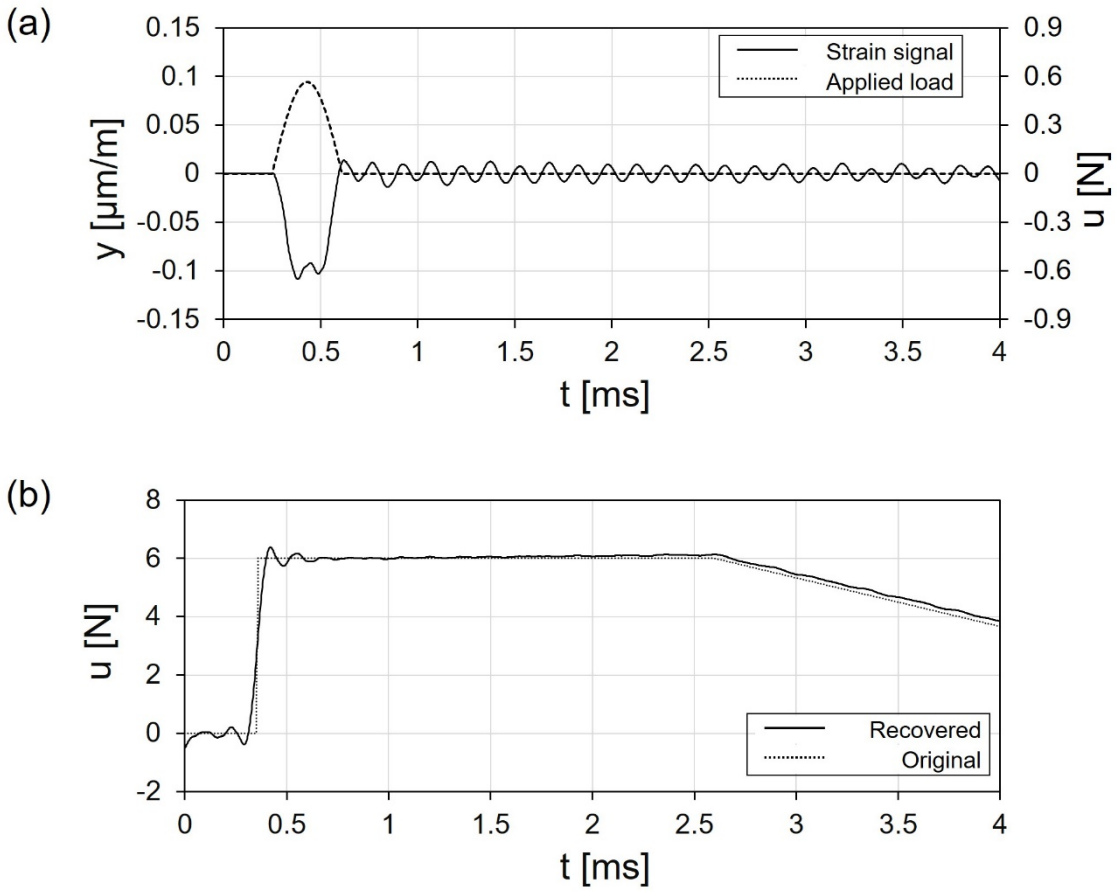

Fig. 5 Drag recovery using pulse load; (a) pulse load response; (b) drag comparison.

4. CONCLUSIONS

In this study, the drag balance based on the stress wave force balance technique was studied, and dynamic calibration was performed through finite element analysis. Based on the results of the pitot pressure measurement of a test facility, aerodynamic drag applied to the test model was assumed, and the resulting strain was simulated. Dynamic calibration was simulated by applying step and pulse loads to the system. The input histories and the resulting strain signals were deconvolved to obtain the impulse response function. Furthermore, the recovered drag values were compared, and the

parameters used for the simulation yielded accurate drag recovery results.

ACKNOWLEDGMENT

This work was supported by the Scramjet Combined Propulsion System Project (No.16-106-501-035) of Republic of Korea.

REFERENCES

Sanderson, S.R. and Simmons, J.M. (1991) “Drag balance for hypervelocity impulse facilities,” *AIAA J.*, **29** (12), 2185-2191.

Paull, A., Stalker, R.J. and Mee, D.J. (1995) “Experiments on supersonic combustion ramjet propulsion in a shock tunnel,” *J. Fluid Mech.*, **296**, 159-183.

Mee, D. (2003a) “Dynamic calibration of force balances for impulse hypersonic facilities,” *Shock Waves*, **12**, 443-455.

Robinson, M.J., Mee, D.J., Tsai, C.Y. and Bakos, R.J. (2004) “Three-component force measurement on a large scramjet in a shock tunnel,” *J. Spacecr. Rocket.*, **41**, 416-425.

Robinson, M.J., Schramm, J.M. and Hannemann, K. (2011) “Design and implementation of an internal stress wave force balance in a shock tunnel,” *CEAS Space J.*, **1**, 45-57.

Vadassery, P., Joshi, D.D., Rolim, T.C. and Lu, F.K. (2013) “Design and testing of an external drag balance for a hypersonic shock tunnel,” *Meas*., **46**, 2110-2117.

Mee, D. (2003b) “Dynamic calibration of force balances,” Dept. of Mechanical Engineering, Univ. of Queensland, Research Report 2002/6.

Park, G. (2013) “Oxygen catalytic recombination on copper oxide in tertiary gas mixtures,” *J. Spacecr. Rocket.,* **50** (3), 540-555.

Cheung, T.M., Schrijer, F.F.J. and Park, G. (2016) “Nitrogen catalytic recombination on copper oxide in tertiary gas mixtures,” *J. Spacecr. Rocket.,* **53** (4), 644-653.

Jo, S.M., Shim, H., Park, G., Kwon, O.J. and Kim, J.G. (2019) “Temperature determination in a shock tube using hydroxyl radical A-X band emission,” Phys. Fluid, **31** (2). 026109.

Yang, Y., Kim, I. and Park, G., (2019) “Experimental and numerical study of oxygen catalytic recombination of SiC-coated material,” *Int. J. Heat Mass Transf.,* **143**, 118510.

Kim, I., Park, G. and Na, J.J. (2019) “Experimental study of surface roughness effect on oxygen catalytic recombination,” *Int. J. Heat Mass Transf*. **138**, 619-922.

Kim, I. and Park, G. (2019) “Experimental study of oxygen catalytic recombination on a smooth surface in a shock tube,” *Appl. Therm. Phys*. **156**, 679-691.

Kim, I., Yang, Y. and Park, G. (2020) “Effect of titanium surface roughness on oxygen catalytic recombination in a shock tube,” *Acta Astronaut*. **166**, 260-269.

Kim, I., Lee, S., Park, G. and Lee, J.K. (2017) “Overview of flow diagnosis in a shock tunnel,” Int. J. of Aeronauti. Space Sci., **18** (3), 157-165.

Lee, S., Song, H., Park, G. and Lee, J.K. (2017) “Freefalling heated sphere in a shock tunnel,” *AIAA J*. **55** (11) 3995-3998.

Lee, S., Song, H. and Park, G. (2020) “Study of strut interference in high-speed flows,” *Exp. Fluids.* **61** (105) 1-20.

Park, S.-H. and Park, G. (2020) “Separation process of multi-spheres in hypersonic flow,” *Adv. Space Res*. **65**, 392-406.

Kim, K. and Park, G. (2020) “Study of test time extension in KAIST shock tunnel,” *J. Propul. Energy*, Under publication.

Hu, Y.H. and Milenkovic, P.L. (1990) “A fast least-square deconvolution algorithm for vocal tract cross section estimation,” *IEEE Trans. Acoust. Speech Signal Process.,* **38**(6), 921-924.